Low-Temperature Atomic Layer Deposition of Cobalt Oxide as an Effective Catalyst for Photoelectrochemical Water-Splitting Devices

Kim, Jiyeon

2017-07-25

Kim , J , Iivonen , T , Hämäläinen , J , Kemell , M , Meinander , K , Mizohata , K , Wang , L , Räisänen , J , Beranek , R , Leskelä , M & Devi , A 2017 , ' Low-Temperature Atomic Layer Deposition of Cobalt Oxide as an Effective Catalyst for Photoelectrochemical Water-Splitting Devices ' , Chemistry of Materials , vol. 29 , no. 14 , pp. 5796-5805 . https://doi.org/10.1021/acs.chemmater.6b05346

http://hdl.handle.net/10138/308511
https://doi.org/10.1021/acs.chemmater.6b05346

acceptedVersion

Low temperature atomic layer deposition of cobalt oxide as an effective catalyst for photoelectrochemical water splitting devices

Jiyeon Kim,[a] Tomi Iivonen,[b] Jani Hämäläinen,[b] Marianna Kemell,[b] Kristoffer Meinander,[c] Kenichiro Mizohata,[c] Lidong Wang,[a] Jyrki Räisänen,[c] Radim Beranek,[a,d]* Markku Leskelä,[b] Anjana Devi[a]*

a) Inorganic Materials Chemistry, Faculty of Chemistry and Biochemistry, Ruhr-University Bochum, Universitätstr. 150, 44801 Bochum, Germany

b) Laboratory of Inorganic Chemistry, Department of Chemistry, University of Helsinki, P.O. Box 55, FI-00014 Helsinki, Finland

c) Division of Materials Physics, Department of Physics, University of Helsinki, P.O. Box 43, FI-00014 Helsinki, Finland

d) Institute of Electrochemistry, Ulm University, Albert-Einstein-Allee 47, 89081 Ulm, Germany

KEYWORDS Cobalt Oxide, Atomic Layer Deposition, Photoelectrochemical Water Splitting Catalysts, Co-catalyst

ABSTRACT: We have developed a low-temperature atomic layer deposition (ALD) process for depositing crystalline and phase pure spinel cobalt oxide (Co_3O_4) films at 120 °C using [Co(^{tBu2}DAD)$_2$] and ozone as co-reagent. X-ray diffraction, UV-Vis spectroscopy, atomic force microscopy, field emission scanning electron microscopy, X-ray photoelectron spectroscopy and time-of-flight elastic recoil detection analysis were performed to characterize the structure and properties of the films. The as-deposited Co_3O_4 films are crystalline with low amount of impurities (<2 % C and <5 % H) despite low deposition temperatures. Deposition of Co_3O_4 onto thin TiO_2 photoanodes (100 nm) for water oxidation resulted in 30 % improvement of photocurrent (after 10 ALD cycles yielding small Co_3O_4 particles) as compared to pristine TiO_2 films), and exhibited no detrimental effects on photocurrent response up to 300 deposition cycles (approximately 35 nm thick films), demonstrating the applicability of the developed ALD process for deposition of effective catalyst particles and layers in photoelectrochemical water-splitting devices.

INTRODUCTION

Nanostructured spinel cobalt(II,III) oxide has been receiving enormous attention due to its various applications in electrochemistry, catalysis, gas sensing, and batteries and energy storage.[1-5] In particular, the use of cobalt oxide as an efficient electrocatalyst for water oxidation[6-9] is of paramount importance as the water oxidation reaction is typically the key kinetic bottleneck in most electrocatalytic and photoelectrocatalytic water splitting systems, which are currently envisaged as highly promising approaches to secure the future supply of low-cost and sustainable energy.[10-17] In general, the activity of electrocatalysts and their applicability in solar-driven water splitting devices depends on various factors, including their composition, morphology, thickness, and optical properties.[7, 9, 12, 18-19] The development of methods allowing for precisely controlled deposition of cobalt oxide films is therefore of crucial importance. Typical methods for the fabrication of cobalt oxides include sol-gel processes,[20-22] spray pyrolysis,[23-26] electrodeposition[7] or physical vapor deposition (PVD)[27-30]. However, in terms of the precise control over the phase and thickness, these methods are outperformed by chemical vapor deposition (CVD) and atomic layer deposition (ALD).[31] Out of these techniques, in particular ALD represents a unique and powerful technique that is capable of depositing films with exceptional conformality, distinct morphology, and phase control on a nanometer scale[28, 32] including deposition of materials over complex-shaped substrates. These features of ALD are of strategic importance for a variety of applications,[33-35] including deposition of light absorbers, protective layers, and catalyst films in photoelectrochemical water splitting devices.[36-42]

Although ALD processes for many metal oxides are known, it is striking that relatively low number of reports are found on the ALD of cobalt oxide. The known processes include deposition of cobalt oxides using cobalt amidinates such as [Co(^{i}PrNCMeN^{i}Pr)$_2$] in a water assisted ALD process,[32, 43] as well as [CoCp$_2$] (Cp = cyclopentadienyl),[15, 44] CCTBA (dicobalthexacarbonyl-tert-butylacetylene),[45] [Co(thd)$_2$] (thd = 2,2,6,6-tetramethylheptan-3,5-dionate)[31] and [Co(acac)$_2$] (acac = acetylacetonate)[34, 46]

with either O_2 plasma or O_3 as the oxygen source. However, these precursors require a high deposition temperature and suffer from low growth rates and incorporation of impurities in the films.[31, 34] Consequently, efforts have been taken to develop cobalt precursors with bidentate chelating ligands such as amidinates.[47] The bidendate effect complements the low thermal stability which can be observed in monodendate comppunds such as amido/imido compounds. Simultaneously, as all nitrogen coordinated compounds, amidinates maintain the low deposition temperatures through the lower bond strength of M–N compared to M–O cases.[48] Notably, Winter et al. have synthesized bis(1,4-di-tert-butyl-1,3-diazadiene) cobalt (II) [Co(^{tBu2}DAD)$_2$] comprising redox non-innocent ligands which normally promise higher redox activity under mild conditions.[49] Recently they have reported a promising low temperature thermal ALD process for the deposition of metallic cobalt (Co^0) using [Co(^{tBu2}DAD)$_2$] and formic acid as a reducing co-reagent.[5]

Herein we report on a low temperature ALD process for the fabrication of phase pure Co_3O_4 thin films, employing [Co(^{tBu2}DAD)$_2$] and ozone as cobalt and oxygen sources, respectively. Moreover, we demonstrate that our low-temperature Co_3O_4 ALD process can be utilized for deposition of effective electrocatalysts onto TiO_2 thin films, which are often regarded as promising protective layers in currently developed photoelectrochemical water splitting devices.[50-53]

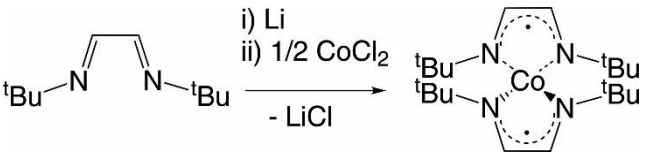

Scheme 1 Synthetic scheme of [Co(^{tBu2}DAD)$_2$][49]

EXPERIMENTAL SECTION

I. Precursor synthesis

[Co(^{tBu2}DAD)$_2$] was synthesized modifying the literature reported procedure (Scheme 1).[49] All manipulations were carried out in an atmosphere of argon purified by Cu catalysts and molecular sieves using standard Schlenk and glove-box techniques. All solvents were dried using an MBraun Solvent Purification System. The crude mixture after the synthesis was sublimed at 60 °C in vacuo (10^{-3} mbar), then the temperature was gradually increased up to 90 °C to remove excess amount of free ligands. Deep dark- green crystals were collected on a cooling finger by slow sublimation (100 °C, 10^{-3} mbar). The purity and the thermal properties were analyzed using elemental analysis, mass spectrometry and thermogravimetric analysis (TGA, EXSTAR 6000 TG/DTA 6200, Seiko Instruments Inc.). The measurements were performed under inert gas atmosphere using nitrogen (99.999 %) at ambient pressure. Approximately 10 mg of samples were filled in aluminum crucibles with a circular opening. The heating rate was 5 °C/min and a nitrogen flow of 300 ml/min was used. For isothermal TG studies, the sample was heated with a rate of 10 °C/min until the desired temperature was reached, then weight loss was measured for 180 min at constant temperature. Electron ionization mass spectra (EI-MS, 70 eV) was measured by a Varian MAT spectrometer.

EI-MS [m/z]: 395.3 $[M]^+$, 380.2 $[M]^+$-CH_3, 338.2 $[M]^+$-$C(CH_3)_3$, 227.1 $[M]^+$-L, 212.1 $[M]^+$-L-CH_3

II. Film deposition

Cobalt oxide thin films were deposited using a hot-wall flow-type ALD reactor (ASM Microchemistry F-120) operated under a nitrogen atmosphere of approximately 5 mbar. Nitrogen (99.999 %) was used as both carrier and purging gas. The carrier gas flow rate used in all depositions was 400 sccm.

Si (100) and soda lime glass cut to 5 × 5 cm^2 pieces were used as substrates. [Co(^{tBu}DAD)$_2$] was sublimed from an open glass boat held inside the reactor at 95 – 100 °C. Ozone was produced from oxygen (99.999 %) using a Weeco Ozomatic Modulator 4 HC Lab Ozone generator (ozone concentration of approximately 100 g/Nm^3) and introduced to the reactor using needle and solenoid valves. The purge time used in all depositions, except with the high aspect ratio (HAR) trench sample, was 2 seconds for both the cobalt precursor and ozone. With the HAR trench sample, 6 second precursor pulses and 10 second purges were used for both the cobalt precursor and ozone. The deposition temperature was varied from 100 – 150 °C. Thin films for photoelectrochemical studies were prepared as follows: 100 nm TiO_2 thin films were deposited on 1.5 x 2.0 cm^2 FTO substrates (Solems TEC7) by applying the $Ti(OMe)_4$ / H_2O ALD process at 275 °C.[54] The TiO_2/Co_3O_4 structures were obtained by applying 10 - 1000 deposition cycles of the Co_3O_4 process at a temperature of 120 °C.

III. Film characterization

All characterizations were conducted using films deposited over 300 cycles (film thickness of approximately 30 nm) on Si (100) substrates unless otherwise noted. All thickness measurements related to saturation studies and the effect of deposition temperature were done on Si (100) with an in situ aluminum oxide layer deposited over 100 cycles using trimethylaluminum (TMA) and ozone (Al_2O_3 film thickness of approximately 10 nm). The purpose of the Al_2O_3 layer was to twofold: I) To produce a reproducible, hydroxylated starting surface[55] for each cobalt oxide film deposition and II) to cover and thus passivate cobalt oxide that would grow on the ALD reactor walls and eventually cause ozone decomposition.[56]

Film thickness was measured with energy dispersive X-ray spectrometry (EDX). The EDX spectra were collected

using an Oxford INCA 350 microanalysis system connected to a Hitachi S-4800 field emission scanning electron microscope (FESEM). Film thicknesses were calculated from the EDX spectra using the GMRfilm software and assuming bulk density values of 6.1 g cm^{-3} for the Co_3O_4 films.[57]

All X-ray diffraction (XRD) measurements were performed in the grazing incidence (GI) geometry using an incident angle of 1 °. Film crystal structure was identified GI-XRD patterns obtained with a PANalytical X'Pert Pro MPD diffractometer. The high temperature XRD (HTXRD) measurements were done using an Anton-Paar HTK1200N oven in both air and nitrogen atmospheres. The nitrogen gas (99.999%) was purified in situ prior to the experiment in an Entegris 35KF-I-4R gas purification system.

Film morphology was studied using both FESEM and atomic force microscopy (AFM). AFM images were captured in tapping mode using a Veeco Multimode V tool equipped with a Nanoscope V controller. Film roughness was calculated as average root mean square (Rq) values from 2 x 2 μm^2 images obtained using Si probes (RTESP, Bruker).

X-ray photoelectron spectra (XPS) were obtained using an Omicron ARGUS spectrometer operated at a pass energy of 20 eV. Samples were illuminated with X-rays emitted from a standard Mg source (K alpha line) at a photon energy of 1253.6 eV. No sputtering was done on the films studied. Binding energies were calibrated using the C 1s peak of ambient hydrocarbons (284.8 eV). Peak fitting was done using the CasaXPS software package.

The time-of-flight elastic recoil detection analysis (ToF-ERDA) measurements were done on films deposited on Si (100) over 1000 cycles using a 50 MeV $^{127}I^{7+}$ ion beam in a setup described in full elsewhere.[58]

UV-Vis transmittance measurements were performed on films deposited on soda lime glass substrates using a Hitachi U2000 spectrophotometer.

IV. Photoelectrochemistry

Photocurrent measurements were carried out using a three electrode setup with a platinum counter electrode and a Ag/AgCl (3M KCl) reference electrode using a SP-300 BioLogic potentiostat. The photoelectrodes were pressed against an O-ring of the cell leaving an irradiated area of 0.5 cm^2. The electrodes were irradiated from the back side (through the FTO glass). The monochromatic wavelength-

resolved photocurrent measurements were performed using a tunable monochromatic light source (Instytut Fotonowy) provided with a 150 W Xenon lamp and a grating monochromator with a bandwidth of 10 nm and SP-300 BioLogic potentiostat. The monochromatic intensities between 300 nm and 800 nm were in the range of 0.16–2.48 mW/cm^2. Appropriate cut-off filters were used in order to eliminate the second-order diffraction radiation. The oxygen evolution was monitored by an OxySense 325i oxygen analyzer in a two-compartment cell, and the electrodes were irradiated by a 150 W Xenon lamp (LOT Oriel) equipped with a KG-3 (Schott) heat-absorbing filter and an AM 1.5 filter. Prior to experiments the electrolyte solutions were purged with argon for 30 minutes.

RESULT AND DISCUSSION

I. Thermal properties of $[Co(^{tBu2}DAD)_2]$

TGA studies of $[Co(^{tBu2}DAD)_2]$ at ambient pressure exhibited onset of volatilization at 160 °C and single-step weight loss with low residues of approximately 4 % (Figure 1). The melting point (175 °C) obtained from the DTA curve is in good agreement with the previously reported value (174 – 175 °C).[49] Isothermal studies at ambient pressure show linear weight loss at 100-120 °C and a constant evaporation rate which indicates capability of sustainable transport of precursor in the ALD reactor conditions over 180 min (Figure 1 (b)). The evaporation rate was determined by the average slope of the isothermal studies and obtained rates were 2.52 µg/min (100 °C), 5.17 µg/min (110 °C) and 11.14 µg/min (120 °C). For the deposition experiments, 100 °C was adopted as the $[Co(^{tBu2}DAD)_2]$

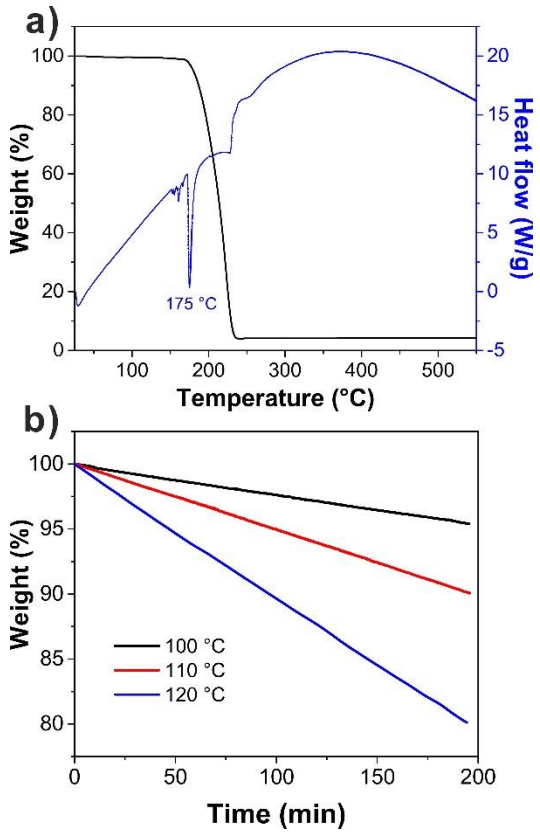

Figure 1 Thermal properties of $[Co(^{tBu2}DAD)_2]$, TGA/DTA (a) and isothermal TG studies (b) measured at 100 – 120 °C.

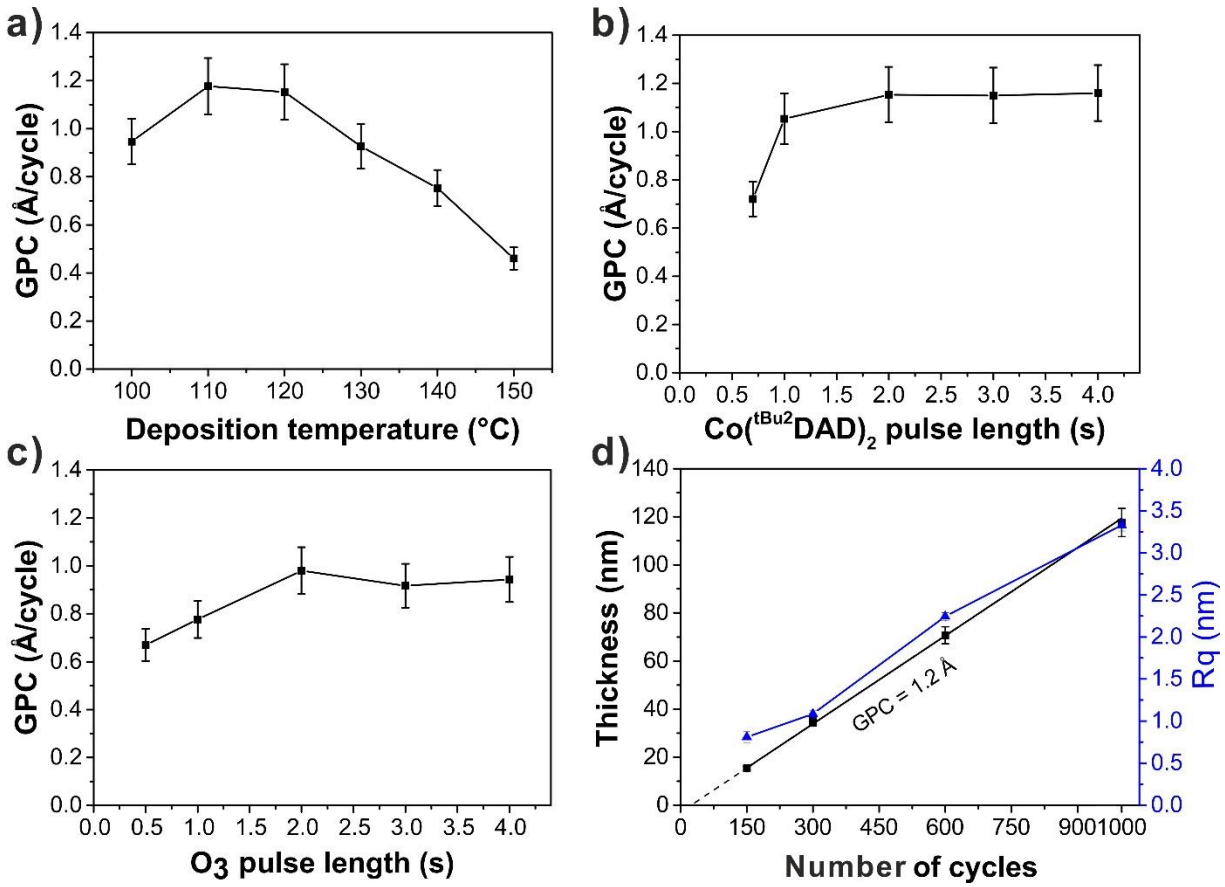

Figure 2 Growth per cycle (GPC) as a function of (a) deposition temperature, (b) [Co(^{tBu2}DAD)$_2$] pulse length, (c) ozone pulse length. (d, black line) Film thickness as a function of number of applied cycles. The R^2 value for a goodness of fit is 0.99967. (d, blue line) Average rms roughness (Rq) as a function of number of applied cycles. Films were grown with 300 cycles using 2 s pulses and purges for both [Co(^{tBu2}DAD)$_2$] and ozone and deposition temperature 120 °C unless otherwise noted.

evaporation temperature. For the depositions performed at temperature of 100 °C, an evaporation temperature of 95 °C was used in order to maintain a thermal gradient between precursor source and substrate chamber.

II. Film deposition

ALD growth of Co_3O_4 was verified by varying the deposition temperature, the precursor pulse lengths of [Co(^{tBu2}DAD)$_2$]/O_3 and the number of deposition cycles. The growth per cycle (GPC) value was investigated as a function of the temperature in the range 100 – 150 °C. As

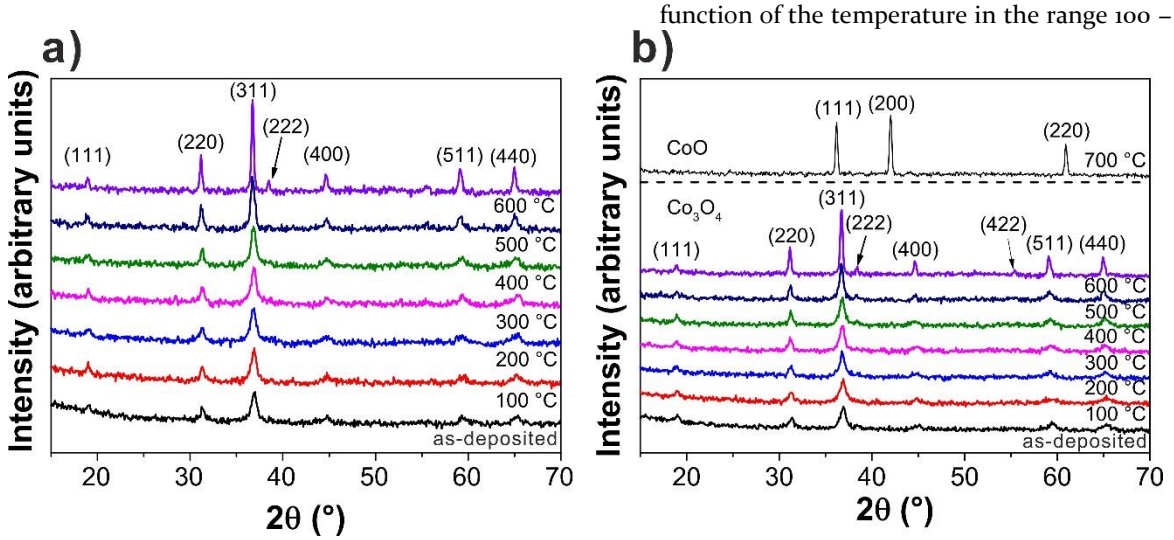

Figure 3 HTXRD patterns of Co_3O_4 films deposited over 1000 cycles at 120 °C in a) air b) nitrogen. The measurement temperature is shown under each diffractogram.

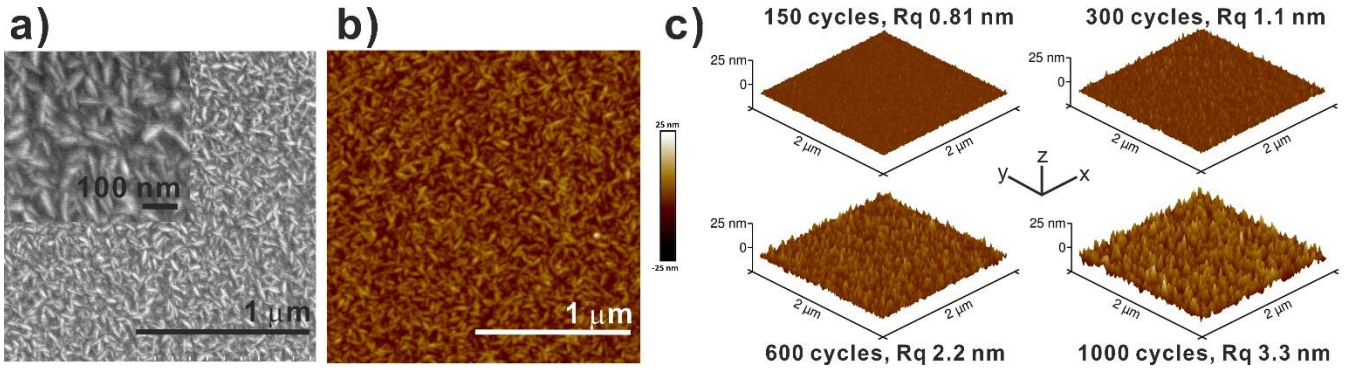

Figure 4 (a) Plane-view SEM and (b) representative AFM images of Co_3O_4 thin film deposited over 1000 cycles at 120 °C. (c) AFM topographs of Co_3O_4 thin films deposited over different cycles at 120 °C and the corresponding Rq values.

can be seen from Figure 2(a), the presence of an ALD window for this process is not obvious. At deposition temperatures of of 110 and 120 C° the GPC value is 1.1 Å.and 1.2 Å, respectively. As the deposition was increased to further, the GPC was found to gradually decrease to 0.5 Å ant 150 °C. In this particular case, the drop in GPC can be attributed to the fact that the rate of ozone decomposition increases rapidly as a function of temperature, especially on the surface of redox active transition metal oxides, such as Co_3O_4.[56, 59] The adverse effect of accelerated ozone decomposition in film growth was also observed when attempting to deposit films on demanding, high aspect ratio (20:1) structures, as completely conformal films in the trench structures could not be produced (Figure S6). Additionally, above 120 °C the deposition of films with fully uniform thickness over entire 5x5 cm^2 substrates could not be achieved. (Figure S3) Therefore, a deposition temperature of 120 °C which resulted fully uniform film on the substrates was adopted for further film growth experiments. (Figure S3 and S4)

Saturation of cobalt oxide film growth was observed after 2 second pulses of Co precursor followed by 2 sec of nitrogen purge, 2 sec of ozone pulse and 2 sec purge which confirmed the self-limiting character at a deposition temperature of 120 °C (Figure 2 (b, c)). Figure 2 (d, black line) substantiates the typical ALD features of saturative growth mode and the linear relation between film thickness and number of applied deposition cycles.[33] The linear fit in Figure 2 (d) does not intersect with the origin, which can be an indication of a nucleation delay. To further evaluate the early stage growth, samples deposited over 10 and 50 cycles were studied using AFM. 10 deposition cycles were found to produce island-like nanoparticles instead of a closed film. After 50 deposition cycles, a closed film formed as evidenced by the homogeneous and smooth surface seen in the AFM image (Figure S11). Additionally, the presence of cobalt oxide after 10 and 50 cycles was confirmed using XPS (Figure S12).

The obtained growth rate of 1.2 Å/cycle at 120 °C is nearly five times higher than previous report on Co_3O_4 ALD (0.25 Å/cycle, $[CoCp_2]/O_3$, ALD window 110 – 300 °C)[31] and it is comparable to recently published results employing diazadienyl cobalt precursor. (1.0 Å/cycle, $Co(^{iPr2}DAD)_2/O_3$ and O_2).[60]

III Film characterization

Structure and morphology

Co_3O_4 films obtained at a deposition temperature of 120 °C were polycrystalline as evidenced by GI-XRD patterns (Figure 3). Diffraction patterns can be assigned to the (111), (220), (311), (222), (400), (511) as well as (440) spinel Co_3O_4 lattice planes,[61] and indicate high crystallinity of

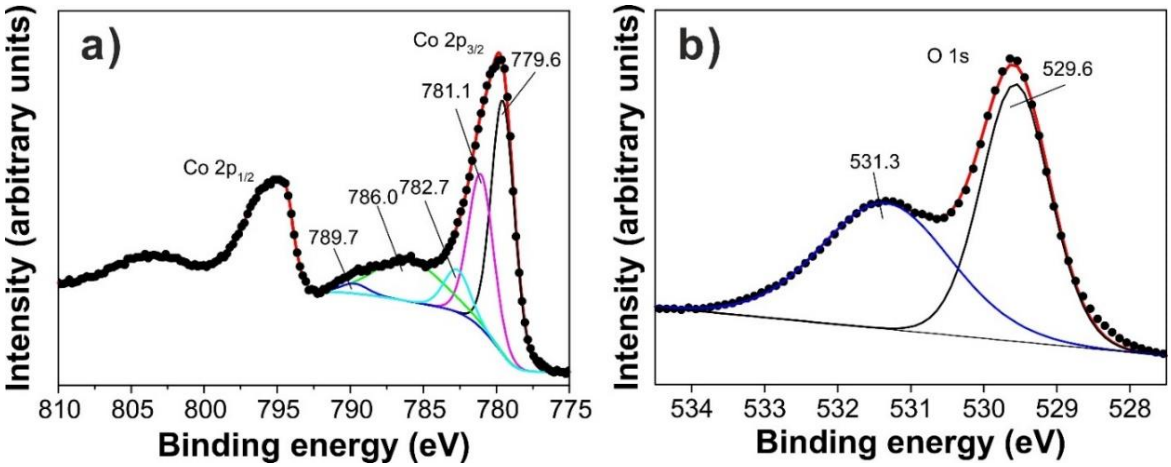

Figure 5 XPS (a) Co 2p and (b) O 1s photoelectron spectra of Co_3O_4 thin film (thickness 110 nm) deposited at 120 °C.

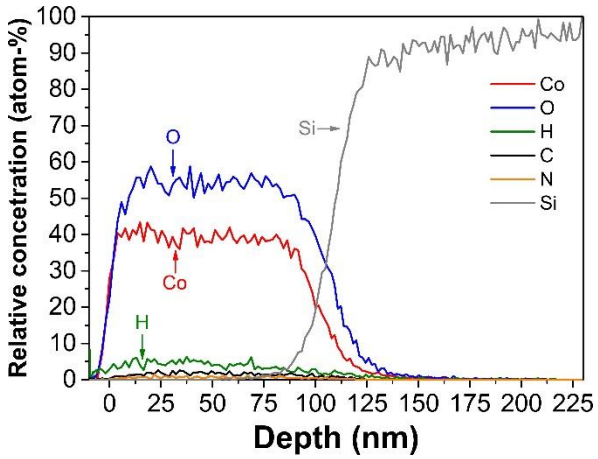

Figure 6 ToF-ERDA depth profile of a Co_3O_4 film deposited over 1000 cycles at 120 °C

Table 1 Elemental compositions of Co_3O_4 films deposited over 1000 cycles at 120 °C

atom-%					
Co	O	H	C	N	Co:O
38.4	54.6	4.8	1.6	0.70	0.70
± 0.4	± 0.6	± 0.5	± 0.1	± 0.1	± 0.2

Co_3O_4 even in as-deposited film (Figure 3). An increase in film crystallinity was observed while measuring HTXRD at both air and nitrogen atmosphere (25 – 700 °C). Upon annealing in oxygen free conditions at 700 °C, the reduction of Co_3O_4 to CoO was observed (Figure 3). The reflections at 700 °C fit to the (111), (200) and (220) periclase CoO lattice planes.[62]

The surface morphology of as-deposited films was studied by both FESEM and AFM. Figure 4 (a,b) shows the SEM and AFM images of Co_3O_4 film grown at 120 °C over 1000 cycles. As can be seen in both figures, homogeneous and well defined nanocrystallites are recognized without any post annealing process. However, due to the low conductivity of the deposited Co_3O_4 films, clear view of the morphology via FESEM was disturbed by the 'charging' effect. Complete view SEM images of Co_3O_4 thin films are shown in the supporting information (Figure S5). Roughness study with equal deposition conditions along the increase of number of cycles is shown in Figure 4 (c). Surface average Rq values rises fairly linear according to the applied number of cycles. (Figure 2 (d, blue line))

Film composition

The surface properties and the chemical composition of as deposited Co_3O_4 films at 120 °C over 1000 cycles were investigated using XPS and ToF-ERDA. XPS was applied to study the chemical states of cobalt and oxygen on the surface of films deposited at 120°C.The survey spectrum of an as-deposited Co_3O_4 film on Si(100) is shown in Figure S7. Core level spectrum of Co 2p in Figure 5 (a) displays spin-orbit splitting into $2p_{1/2}$ and $2p_{3/2}$ components with plateau shake-up peaks representing mixed oxidation state of $Co^{2+/3+}$. The satellite line enables to distinguish between Co^{2+} and Co^{3+} chemical states whereas pure Co^{2+} has a projecting shake-up peak in both area of 786 and 790 eV while pure Co^{3+} shows mainly in the area of 790 eV.[63] Since, both components contain qualitatively identical chemical information, the higher intensity peak $2p_{3/2}$ was chosen for curve fitting and used for qualitative analysis. Binding energy peaks at

779.6 and 781.1 eV agree with the presence of Co^{3+} and Co^{2+} species, respectively and their shake-up peaks appear at 786.0 and 789.7 eV.[63-65] The peak at 782.7 eV suggests that there is $Co(OH)_2$ species present on the surface.[63] O 1s peak at 531.3 eV is ascribed to the lattice oxygen in the Co_3O_4 spinel structure while the peak at 529.6 eV is mainly related to hydroxyl group from $Co(OH)_2$ species. [63]

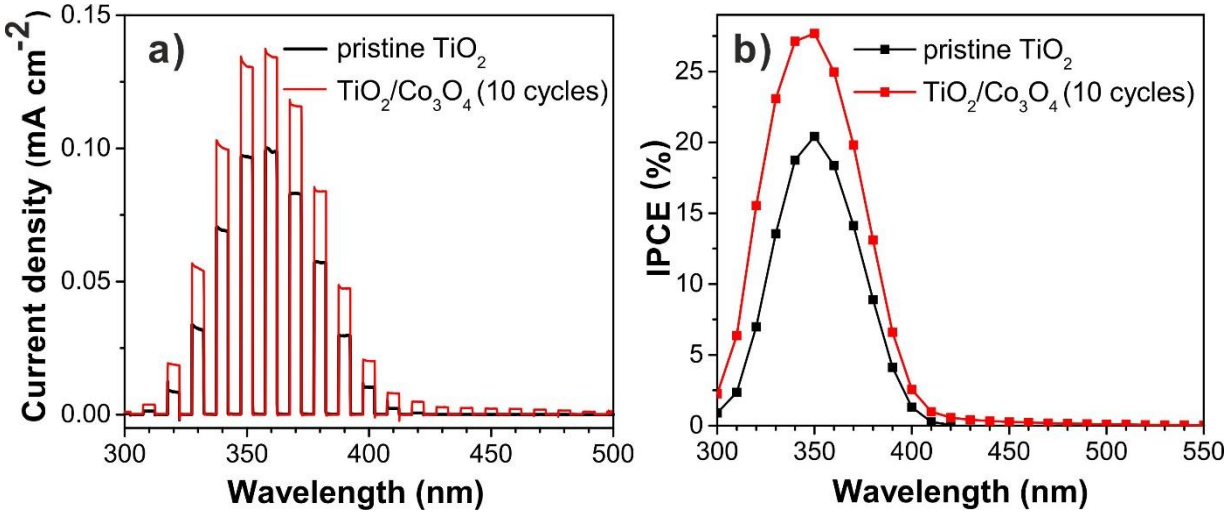

Figure 7 Photocurrent transients under intermittent irradiation at different wavelengths (a) and the corresponding photoaction spectrum (b) recorded in KOH (0.1 M) at 1.48 V vs. RHE at TiO_2 (100 nm) and TiO_2/Co_3O_4 (10 cycles) photoanodes.

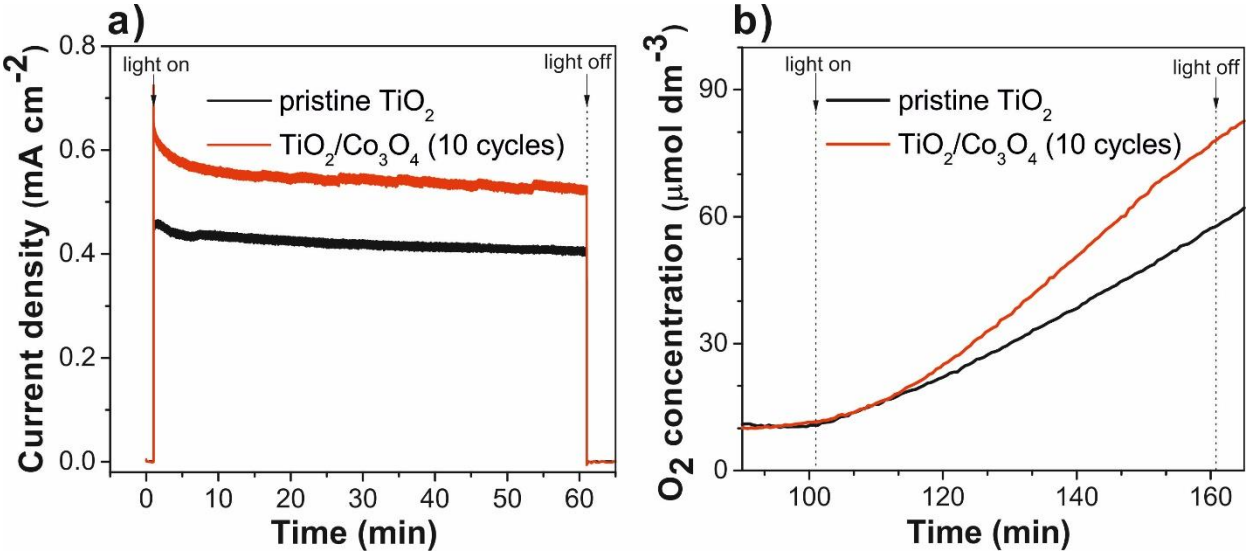

Figure 8 Photoelectrocatalytic properties of TiO_2 (100 nm) and TiO_2/Co_3O_4 (10 cycles) photoanodes: (a) photocurrents (a) and oxygen evolution (b) during 1 hour irradiation by simulated sunlight (Xenon lamp, AM1.5 filter, 100 mW/cm²) in borate buffer solution (0.1 M; pH 9.2) at 1.25 V vs. RHE.

To further study the film composition, ToF-ERDA was used to create a depth profile and to determine the Co:O ratio. ToF-ERDA is one of the few methods that can be used to quantitatively detect light elements such as hydrogen[58, 66] and it overcomes the intrinsic limitation of Rutherford Backscattering Spectrometry (RBS),[67] which is why it is an excellent technique to complement XPS measurements. The ToF-ERDA measurements revealed that the films contain < 5 % hydrogen. Furthermore, the amount of hydrogen was found to increase towards the surface, which can explain the formation of the surface hydroxyls detected by XPS (Figure 6, Table 1).

IV Photoelectrochemical properties

Cobalt oxides are highly efficient electrocatalysts for the oxygen evolution reaction which is a key process in all solar-driven water splitting devices.[6] Notably, the most active cobalt-based electrocatalysts are known to be structurally equivalent to a disordered form of heterogenite, CoO(OH).[7, 9, 68-69] The above mentioned concomitant presence of partially hydroxylated Co^{2+} and Co^{3+} at the surface of our films is significant, as it suggests that formation of CoO(OH) is likely to occur under electrocatalytic conditions.[9] In order to examine the suitability of our ALD-grown films for solar water splitting devices, we applied 10 – 1000 deposition cycles of Co_3O_4 onto a 100 nm thick TiO_2 layer deposited by ALD on FTO glass substrates (Figure S11). Obviously, the prospects of using TiO2 as a light absorber for water splitting are very limited since TiO_2 is photoactive only under UV light irradiation due to its large bandgap (3.2 eV / 390 nm). However, the here investigated well-defined TiO_2/Co_3O_4 thin film architectures are highly relevant for future photoelectrochemical water splitting systems since TiO_2 films are currently being intensely investigated as effective protection layers for low-gap semiconductors like Si, GaAs, GaP or CdTe which are normally prone to severe photocorrosion.[50-53, 70-71]

Among the TiO_2/Co_3O_4 structures with different amount of Co_3O_4, the sample after 10 ALD cycles showed the best photoelectrocatalytic performance. In both the photoaction spectra (Figure 7) and under polychromatic irradiation by simulated solar light (Figure 8), the presence of Co_3O_4 improved the photocurrent response by approximately 30% as compared to pristine TiO_2. Notably, after only 10 ALD cycles, cobalt oxide particles rather than closed films are expected to be deposited. Indeed, this has been confirmed by AFM and XPS investigations (Figures S10 and S11). However, it should be noted that photocurrents similar or even slightly enhanced as compared to pristine TiO_2 photocurrents are observed even after 300 ALD cycles (Figure S10), corresponding to a closed Co_3O_4 layer of a thickness of approximately 35 nm. Importantly, this demonstrates that the ALD-grown Co_3O_4 does not induce any undesirable surface defect states in TiO_2 which would lead to enhanced surface recombination. Clearly, the holes are effectively extracted from TiO_2 into Co_3O_4, which enhances the charge separation and in turn results in the observed increase of photocurrent.[72] After 500 ALD cycles the photocurrents decrease slightly (Figure S10), most probably due to problems with hole diffusion through thicker Co_3O_4 films. This is corroborated by photocurrent transients after 1000 ALD cycles showing a spike-like behavior (Figure S10), which is indicative of fast recombination due to hole accumulation in the surface Co_3O_4 layer. [73-74]

It cannot be excluded that cobalt oxide can also act beneficially by passivating surface states in TiO_2, as has been recently suggested in case of photoanodes based on Fe_2O_3 or $BiVO_4$.[75-77] In this context, it should be noted that the

photoholes in pristine TiO_2 possess a highly positive potential and do not necessarily require the presence of a co-catalyst to induce complete water oxidation to dioxygen under photoelectrochemical conditions. Accordingly, as expected, the enhancement of the oxygen evolution rate (Figure 8 (b)) is comparable to the enhancement of photocurrent, without any significant change in the Faradaic efficiency of oxygen evolution. We note that the oxygen evolution measurements have been performed in borate buffer (pH 9.2) in order to avoid problems with the stability of the oxygen sensor. Moreover, recent investigations have shown a superior stability of cobalt-based co-catalysts in borate electrolytes.[78] At any rate, the fact that, under optimized conditions (number of cycles), the ALD-grown Co_3O_4 particles and layers on TiO_2 do not diminish the photocurrents is highly significant. Firstly, it demonstrates that our low-temperature ALD process can be utilized for deposition of cobalt oxide electrocatalysts onto TiO_2-based light absorbers in various photocatalytic and photoelectrochemical systems.[79] Secondly, it suggests that the ALD process is applicable also for deposition of effective cobalt oxide electrocatalytic films onto TiO_2 protective layers on low-bandgap semiconductors like Si, GaAs, GaP or CdTe which play a pivotal role in currently developed photoanodes for tandem water-splitting devices.[50-53] Obviouly, in any specific photoelectrocatalytic application the thickness of the electrocatalyst layer must be optimized depending on the light management (frontside vs backside illumination), taking into account the transmittance of Co_3O_4 films of various thickness in order to avoid the parasitic light absorption by the electrocatalyst (Figure S10).

CONCLUSION

To summarize, we have demonstrated the atomic layer deposition of spinel cobalt oxide using [Co(^{tBu2}DAD)$_2$] with ozone as cobalt and oxygen sources, respectively in a low temperature process (120 °C). The obtained Co_3O_4 thin films turned out to be uniform, crystalline, phase pure and include only low carbon and hydrogen contamination even without a post-annealing treatment. Finally, we demonstrated that our ALD process allows for the deposition of effective Co_3O_4 electrocatalysts onto TiO_2 films, resulting in improved photoconversion efficiency. Given the excellent uniformity of ALD-grown layers and the prominent role of thin TiO_2 films as protective layers in photoelectrodes, we expect that our low-temperature ALD process will find immediate application in fabrication of various devices for solar water splitting.

ASSOCIATED CONTENT

EI, AFM and XPS; as well as further details for supporting information is available free of charge via the Internet at http://pubs.acs.org.

AUTHOR INFORMATION

Corresponding Authors

*E-mail: anjana.devi@rub.de; radim.beranek@uni-ulm.de

Author Contributions

J. Kim and T. Iivonen contributed equally on the manuscript.

Notes

The authors declare no competing financial interest.

ACKNOWLEDGMENT

Financial support by the EU-FP7 Grant "4G-PHOTOCAT" (Grant No. 309636), DFG (BE 5102/4-1 and DE 790/12-1) and The Finnish Centre of Excellence in Atomic Layer Deposition (Academy of Finland) are gratefully acknowledged. T. Iivonen wishes to acknowledge the COST action MP1402 HERALD for support. J. Kim is thankful for support by the Ruhr-Universität Bochum Research School (http://www.research.school.rub.de). Miika Mattinen is acknowledged for his assistance with the AFM studies.

REFERENCES

1. Švegl, F.; Orel, B.; Hutchins, M. G.; Kalcher, K., Structural and Spectroelectrochemical Investigations of Sol-Gel Derived Electrochromic Spinel Co_3O_4 Films. *J. Electrochem. Soc.* **1996,** *143*, 1532-1539.
2. Ando, M.; Kobayashi, T.; Iijima, S.; Haruta, M., Optical recognition of CO and H_2 by use of gas-sensitive Au-Co_3O_4 composite films. *J. Mater. Chem.* **1997,** *7*, 1779-1783.
3. Li, W. Y.; Xu, L. N.; Chen, J., Co_3O_4 Nanomaterials in Lithium-Ion Batteries and Gas Sensors. *Adv. Funct. Mater.* **2005,** *15*, 851-857.
4. Bekermann, D.; Gasparotto, A.; Barreca, D.; Maccato, C.; Comini, E.; Sada, C.; Sberveglieri, G.; Devi, A.; Fischer, R. A., Co_3O_4/ZnO Nanocomposites: From Plasma Synthesis to Gas Sensing Applications. *ACS Appl. Mater. Interfaces* **2012,** *4*, 928-934.
5. Klesko, J. P.; Kerrigan, M. M.; Winter, C. H., Low Temperature Thermal Atomic Layer Deposition of Cobalt Metal Films. *Chem. Mater.* **2016,** *28*, 700-703.
6. Harriman, A.; Pickering, I. J.; Thomas, J. M.; Christensen, P. A., Metal oxides as heterogeneous catalysts for oxygen evolution under photochemical conditions. *J. Chem. Soc. Faraday Trans.* **1988,** *84*, 2795-2806.
7. Kanan, M. W.; Nocera, D. G., In Situ Formation of an Oxygen-Evolving Catalyst in Neutral Water Containing Phosphate and Co^{2+}. *Science* **2008,** *321*, 1072-1075.
8. Yang, J.; Walczak, K.; Anzenberg, E.; Toma, F. M.; Yuan, G.; Beeman, J.; Schwartzberg, A.; Lin, Y.; Hettick, M.; Javey, A.; Ager, J. W.; Yano, J.; Frei, H.; Sharp, I. D., Efficient and Sustained Photoelectrochemical Water Oxidation by Cobalt Oxide/Silicon Photoanodes with Nanotextured Interfaces. *J. Am. Chem. Soc.* **2014,** *136*, 6191-6194.
9. Bergmann, A.; Martinez-Moreno, E.; Teschner, D.; Chernev, P.; Gliech, M.; de Araújo, J. F.; Reier, T.; Dau, H.; Strasser, P., Reversible amorphization and the catalytically active state of crystalline Co_3O_4 during oxygen evolution. *Nat. Commun.* **2015,** *6*, 8625.
10. Lewis, N. S.; Nocera, D. G., Powering the planet: Chemical challenges in solar energy utilization. *Proc. Natl. Acad. Sci.* **2006,** *103*, 15729-15735.

11. Dau, H.; Limberg, C.; Reier, T.; Risch, M.; Roggan, S.; Strasser, P., The Mechanism of Water Oxidation: From Electrolysis via Homogeneous to Biological Catalysis. *ChemCatChem* **2010,** *2*, 724-761.
12. Trotochaud, L.; Mills, T. J.; Boettcher, S. W., An Optocatalytic Model for Semiconductor − Catalyst Water-Splitting Photoelectrodes Based on In Situ Optical Measurements on Operational Catalysts. *J. Phys. Chem. Lett.* **2013,** *4*, 931-935.
13. Yang, J.; Wang, D.; Han, H.; Li, C., Roles of Cocatalysts in Photocatalysis and Photoelectrocatalysis. *Acc. Chem. Res.* **2013,** *46*, 1900-1909.
14. Peter, L. M., Photoelectrochemical Water Splitting. A Status Assessment. *Electroanalysis* **2015,** *27*, 864-871.
15. Ager, J. W.; Shaner, M. R.; Walczak, K. A.; Sharp, I. D.; Ardo, S., Experimental demonstrations of spontaneous, solar-driven photoelectrochemical water splitting. *Energy Environ. Sci.* **2015,** *8*, 2811-2824.
16. Zhou, X.; Shen, X.; Xia, Z.; Zhang, Z.; Li, J.; Ma, Y.; Qu, Y., Hollow Fluffy Co_3O_4 Cages as Efficient Electroactive Materials for Supercapacitors and Oxygen Evolution Reaction. *ACS Appl. Mater. Interfaces* **2015,** *7*, 20322-20331.
17. Chua, C. S.; Ansovini, D.; Lee, C. J. J.; Teng, Y. T.; Ong, L. T.; Chi, D.; Hor, T. S. A.; Raja, R.; Lim, Y.-F., The effect of crystallinity on photocatalytic performance of Co_3O_4 water-splitting cocatalysts. *Phys. Chem. Chem. Phys.* **2016,** *18*, 5172-5178.
18. Lin, F.; Boettcher, S. W., Adaptive semiconductor/electrocatalyst junctions in water-splitting photoanodes. *Nat. Mater.* **2014,** *13*, 81-86.
19. Nellist, M. R.; Laskowski, F. A. L.; Lin, F.; Mills, T. J.; Boettcher, S. W., Semiconductor−Electrocatalyst Interfaces: Theory, Experiment, and Applications in Photoelectrochemical Water Splitting. *Acc. Chem. Res.* **2016,** *49*, 733-740.
20. Barrera, E.; Viveros, T.; Avila, A.; Quintana, P.; Morales, M.; Batina, N., Cobalt oxide films grown by a dipping sol-gel process. *Thin Solid Films* **1999,** *346*, 138-144.
21. Armelao, L.; Barreca, D.; Gross, S.; Martucci, A.; Tieto, M.; Tondello, E., Cobalt oxide-based films: sol−gel synthesis and characterization. *J. Non-Cryst. Solids* **2001,** *293*−*295*, 477-482.
22. Quinlan, F. T.; Vidu, R.; Predoana, L.; Zaharescu, M.; Gartrner, M.; Groza, J.; Stroeve, P., Lithium Cobalt Oxide ($LiCoO_2$) Nanocoatings by Sol–Gel Methods. *Ind. Eng. Chem. Res.* **2004,** *43*, 2468-2477.
23. Athey, P. R.; Urban, F. K.; Tabet, M. F.; McGahan, W. A., Optical properties of cobalt oxide films deposited by spray pyrolysis. *J. Vac. Sci. Technol., A* **1996,** *14*, 685-692.
24. Shinde, V. R.; Mahadik, S. B.; Gujar, T. P.; Lokhande, C. D., Supercapacitive cobalt oxide (Co_3O_4) thin films by spray pyrolysis. *Appl. Surf. Sci.* **2006,** *252*, 7487-7492.
25. Louardi, A.; Rmili, A.; Ouachtari, F.; Bouaoud, A.; Elidrissi, B.; Erguig, H., Characterization of cobalt oxide thin films prepared by a facile spray pyrolysis technique using perfume atomizer. *J. Alloy. Compd.* **2011,** *509*, 9183-9189.
26. Abbas, T. A.-H.; Slewa, L. H.; Khizir, H. A.; Kakil, S. A., Synthesis of cobalt oxide (Co_3O_4) thin films by electrostatic spray pyrolysis technique (ESP). *J. Mater. Sci. Mater. Electron.* **2016**, 1-7.
27. Meyer, W.; Biedermann, K.; Gubo, M.; Hammer, L.; Heinz, K., Surface structure of polar Co_3O_4 (111) films grown epitaxially on Ir(100)-(1 × 1). *J. Phys. Condens. Matter* **2008,** *20*, 265011.
28. Johnson, R. W.; Hultqvist, A.; Bent, S. F., A brief review of atomic layer deposition: from fundamentals to applications. *Mater. Today* **2014,** *17*, 236-246.
29. Mazzi, A.; Bazzanella, N.; Orlandi, M.; Edla, R.; Patel, N.; Fernandes, R.; Miotello, A., Physical vapor deposition of mixed-metal oxides based on Fe, Co and Ni as water oxidation catalysts. *Mater. Sci. Semicond. Process.* **2016,** *42, Part 1*, 155-158.
30. Xu, T.; Schwarz, M.; Werner, K.; Mohr, S.; Amende, M.; Libuda, J., Structure-Dependent Anchoring of Organic Molecules to Atomically Defined Oxide Surfaces: Phthalic Acid on Co_3O_4(111), CoO(100), and CoO(111). *Chem. Eur. J.* **2016,** *22*, 5384-5396.
31. Klepper, K. B.; Nilsen, O.; Fjellvåg, H., Growth of thin films of Co_3O_4 by atomic layer deposition. *Thin Solid Films* **2007,** *515*, 7772-7781.
32. Ngo, T. Q.; Posadas, A.; Seo, H.; Hoang, S.; McDaniel, M. D.; Utess, D.; Triyoso, D. H.; Buddie Mullins, C.; Demkov, A. A.; Ekerdt, J. G., Atomic layer deposition of photoactive CoO/$SrTiO_3$ and CoO/TiO_2 on Si(001) for visible light driven photoelectrochemical water oxidation. *J. Appl. Phys.* **2013,** *114*, 084901.
33. Leskelä, M.; Ritala, M., Atomic Layer Deposition Chemistry: Recent Developments and Future Challenges. *Angew. Chem. Int. Ed.* **2003,** *42*, 5548-5554.
34. Backman, L. B.; Rautiainen, A.; Lindblad, M.; Krause, A. O. I., The interaction of cobalt species with alumina on Co/Al_2O_3 catalysts prepared by atomic layer deposition. *Appl. Catal., A* **2009,** *360*, 183-191.
35. Barreca, D.; Devi, A.; Fischer, R. A.; Bekermann, D.; Gasparotto, A.; Gavagnin, M.; Maccato, C.; Tondello, E.; Bontempi, E.; Depero, L. E.; Sada, C., Strongly oriented Co_3O_4 thin films on MgO(100) and $MgAl_2O_4$(100) substrates by PE-CVD. *CrystEngComm* **2011,** *13*, 3670-3673.
36. Liu, R.; Lin, Y.; Chou, L.-Y.; Sheehan, S. W.; He, W.; Zhang, F.; Hou, H. J. M.; Wang, D., Water Splitting by Tungsten Oxide Prepared by Atomic Layer Deposition and Decorated with an Oxygen-Evolving Catalyst. *Angew. Chem. Int. Ed.* **2011,** *50*, 499-502.
37. Paracchino, A.; Laporte, V.; Sivula, K.; Grätzel, M.; Thimsen, E., Highly active oxide photocathode for photoelectrochemical water reduction. *Nat. Mater.* **2011,** *10*, 456-461.
38. Morales-Guio, C. G.; Tilley, S. D.; Vrubel, H.; Grätzel, M.; Hu, X., Hydrogen evolution from a copper(I) oxide photocathode coated with an amorphous molybdenum sulphide catalyst. *Nat. Commun.* **2014,** *5*, 3059.
39. Young, K. M. H.; Hamann, T. W., Enhanced photocatalytic water oxidation efficiency with $Ni(OH)_2$ catalysts deposited on [small alpha]-Fe_2O_3 via ALD. *Chem. Commun.* **2014,** *50*, 8727-8730.
40. Steier, L.; Luo, J.; Schreier, M.; Mayer, M. T.; Sajavaara, T.; Grätzel, M., Low-Temperature Atomic Layer Deposition of Crystalline and Photoactive Ultrathin Hematite Films for Solar Water Splitting. *ACS Nano* **2015,** *9*, 11775-11783.
41. Hajibabaei, H.; Zandi, O.; Hamann, T. W., Tantalum nitride films integrated with transparent conductive oxide substrates via atomic layer deposition for photoelectrochemical water splitting. *Chem. Sci.* **2016,** *7*, 6760-6767.

42. Yang, J.; Cooper, J. K.; Toma, F. M.; Walczak, K. A.; Favaro, M.; Beeman, J. W.; Hess, L. H.; Wang, C.; Zhu, C.; Gul, S.; Yano, J.; Kisielowski, C.; Schwartzberg, A.; Sharp, I. D., A multifunctional biphasic water splitting catalyst tailored for integration with high-performance semiconductor photoanodes. *Nat. Mater.* **2017,** *16*, 335-341.
43. Lim, B. S.; Rahtu, A.; Gordon, R. G., Atomic layer deposition of transition metals. *Nat. Mater.* **2003,** *2*, 749-754.
44. Lichterman, M. F.; Shaner, M. R.; Handler, S. G.; Brunschwig, B. S.; Gray, H. B.; Lewis, N. S.; Spurgeon, J. M., Enhanced Stability and Activity for Water Oxidation in Alkaline Media with Bismuth Vanadate Photoelectrodes Modified with a Cobalt Oxide Catalytic Layer Produced by Atomic Layer Deposition. *J. Phys. Chem. Lett.* **2013,** *4*, 4188-4191.
45. Han, B.; Choi, K. H.; Park, K.; Han, W. S.; Lee, W.-J., Low-Temperature Atomic Layer Deposition of Cobalt Oxide Thin Films Using Dicobalt Hexacarbonyl tert-Butylacetylene and Ozone. *Electrochem. Solid State Lett.* **2011,** *15*, D14-D17.
46. Taheri Najafabadi, A.; Khodadadi, A. A.; Parnian, M. J.; Mortazavi, Y., Atomic layer deposited Co/ɣ-Al_2O_3 catalyst with enhanced cobalt dispersion and Fischer – Tropsch synthesis activity and selectivity. *Appl. Catal., A* **2016,** *511*, 31-46.
47. Lim, B. S.; Rahtu, A.; Park, J.-S.; Gordon, R. G., Synthesis and Characterization of Volatile, Thermally Stable, Reactive Transition Metal Amidinates. *Inorg. Chem.* **2003,** *42*, 7951-7958.
48. Barry, S. T., Amidinates, guanidinates and iminopyrrolidinates: Understanding precursor thermolysis to design a better ligand. *Coord. Chem. Rev.* **2013,** *257*, 3192-3201.
49. Knisley, T. J.; Saly, M. J.; Heeg, M. J.; Roberts, J. L.; Winter, C. H., Volatility and High Thermal Stability in Mid- to Late-First-Row Transition-Metal Diazadienyl Complexes. *Organometallics* **2011,** *30*, 5010-5017.
50. Chen, Y. W.; Prange, J. D.; Duehnen, S.; Park, Y.; Gunji, M.; Chidsey, C. E. D.; McIntyre, P. C., Atomic layer-deposited tunnel oxide stabilizes silicon photoanodes for water oxidation. *Nat. Mater.* **2011,** *10*, 539-544.
51. Scheuermann, A. G.; Prange, J. D.; Gunji, M.; Chidsey, C. E. D.; McIntyre, P. C., Effects of catalyst material and atomic layer deposited TiO_2 oxide thickness on the water oxidation performance of metal-insulator-silicon anodes. *Energy Environ. Sci.* **2013,** *6*, 2487-2496.
52. Hu, S.; Shaner, M. R.; Beardslee, J. A.; Lichterman, M.; Brunschwig, B. S.; Lewis, N. S., Amorphous TiO_2 coatings stabilize Si, GaAs, and GaP photoanodes for efficient water oxidation. *Science* **2014,** *344*, 1005-1009.
53. Lichterman, M. F.; Carim, A. I.; McDowell, M. T.; Hu, S.; Gray, H. B.; Brunschwig, B. S.; Lewis, N. S., Stabilization of n-cadmium telluride photoanodes for water oxidation to O_2(g) in aqueous alkaline electrolytes using amorphous TiO_2 films formed by atomic-layer deposition. *Energy Environ. Sci.* **2014,** *7*, 3334-3337.
54. Pore, V.; Rahtu, A.; Leskelä, M.; Ritala, M.; Sajavaara, T.; Keinonen, J., Atomic Layer Deposition of Photocatalytic TiO_2 Thin Films from Titanium Tetramethoxide and Water. *Chem. Vap. Deposition* **2004,** *10*, 143-148.
55. Goldstein, D. N.; McCormick, J. A.; George, S. M., Al_2O_3 Atomic Layer Deposition with Trimethylaluminum and Ozone Studied by in Situ Transmission FTIR Spectroscopy and Quadrupole Mass Spectrometry. *J. Phys. Chem. C* **2008,** *112*, 19530-19539.
56. Knoops, H. C. M.; Elam, J. W.; Libera, J. A.; Kessels, W. M. M., Surface Loss in Ozone-Based Atomic Layer Deposition Processes. *Chem. Mater.* **2011,** *23*, 2381-2387.
57. Waldo, R. A., An iteration procedure to calculate film compositions and thicknesses in electron-probe microanalysis. *Microbeam Anal.* **1988,** *23rd*, 310-14.
58. Jokinen, J.; Keinonen, J.; Tikkanen, P.; Kuronen, A.; Ahlgren, T.; Nordlund, K., Comparison of TOF-ERDA and nuclear resonance reaction techniques for range profile measurements of keV energy implants. *Nucl. Instr. Meth. Phys. Res.* **1996,** *119*, 533-542.
59. Li, W.; Gibbs, G. V.; Oyama, S. T., Mechanism of Ozone Decomposition on a Manganese Oxide Catalyst. 1. In Situ Raman Spectroscopy and Ab Initio Molecular Orbital Calculations. *J. Am. Chem. Soc.* **1998,** *120*, 9041-9046.
60. Han, B.; Park, J.-M.; Choi, K. H.; Lim, W.-K.; Mayangsari, T. R.; Koh, W.; Lee, W.-J., Atomic layer deposition of stoichiometric Co_3O_4 films using bis(1,4-di-iso-propyl-1,4-diazabutadiene) cobalt. *Thin Solid Films* **2015,** *589*, 718-722.
61. Will, G.; Masciocchi, N.; Parrish, W.; Hart, M., Refinement of simple crystal structures from synchrotron radiation powder diffraction data. *J. Appl. Crystallogr.* **1987,** *20*, 394-401.
62. Liu, J. F.; Yin, S.; Wu, H. P.; Zeng, Y. W.; Hu, X. R.; Wang, Y. W.; Lv, G. L.; Jiang, J. Z., Wurtzite-to-Rocksalt Structural Transformation in Nanocrystalline CoO. *J. Phys. Chem. B* **2006,** *110*, 21588-21592.
63. Yang, J.; Liu, H.; Martens, W. N.; Frost, R. L., Synthesis and Characterization of Cobalt Hydroxide, Cobalt Oxyhydroxide, and Cobalt Oxide Nanodiscs. *J. Phys. Chem. C* **2010,** *114*, 111-119.
64. Biesinger, M. C.; Payne, B. P.; Grosvenor, A. P.; Lau, L. W. M.; Gerson, A. R.; Smart, R. S. C., Resolving surface chemical states in XPS analysis of first row transition metals, oxides and hydroxides: Cr, Mn, Fe, Co and Ni. *Appl. Surf. Sci.* **2011,** *257*, 2717-2730.
65. Li, J.; Lu, G.; Wu, G.; Mao, D.; Guo, Y.; Wang, Y.; Guo, Y., Effect of TiO_2 crystal structure on the catalytic performance of Co_3O_4/TiO_2 catalyst for low-temperature CO oxidation. *Catal. Sci. Tech.* **2014,** *4*, 1268-1275.
66. Putkonen, M.; Sajavaara, T.; Niinistö, L.; Keinonen, J., Analysis of ALD-processed thin films by ion-beam techniques. *Anal. Bioanal. Chem.* **2005,** *382*, 1791-1799.
67. Donders, M. E.; Knoops, H. C. M.; van, M. C. M.; Kessels, W. M. M.; Notten, P. H. L., Remote Plasma Atomic Layer Deposition of Co3O4 Thin Films. *J. Electrochem. Soc.* **2011,** *158*, G92-G96.
68. Kanan, M. W.; Yano, J.; Surendranath, Y.; Dincă, M.; Yachandra, V. K.; Nocera, D. G., Structure and Valency of a Cobalt–Phosphate Water Oxidation Catalyst Determined by in Situ X-ray Spectroscopy. *J. Am. Chem. Soc.* **2010,** *132*, 13692-13701.
69. Risch, M.; Ringleb, F.; Kohlhoff, M.; Bogdanoff, P.; Chernev, P.; Zaharieva, I.; Dau, H., Water oxidation by amorphous cobalt-based oxides: in situ tracking of redox transitions and mode of catalysis. *Energy Environ. Sci.* **2015,** *8*, 661-674.
70. Liu, R.; Zheng, Z.; Spurgeon, J.; Yang, X., Enhanced photoelectrochemical water-splitting performance of semiconductors by surface passivation layers. *Energy & Environmental Science* **2014,** *7*, 2504-2517.
71. Yang, X.; Liu, R.; He, Y.; Thorne, J.; Zheng, Z.; Wang, D., Enabling practical electrocatalyst-assisted photoelectron-

chemical water splitting with earth abundant materials. *Nano Research* **2015,** *8*, 56-81.
72. Ramakrishnan, V.; Kim, H.; Park, J.; Yang, B., Cobalt oxide nanoparticles on TiO_2 nanorod/FTO as a photoanode with enhanced visible light sensitization. *RSC Adv.* **2016,** *6*, 9789-9795.
73. Peter, L. M., Dynamic aspects of semiconductor photoelectrochemistry. *Chem. Rev.* **1990,** *90*, 753-769.
74. Bledowski, M.; Wang, L.; Neubert, S.; Mitoraj, D.; Beranek, R., Improving the Performance of Hybrid Photoanodes for Water Splitting by Photodeposition of Iridium Oxide Nanoparticles. *The Journal of Physical Chemistry C* **2014,** *118*, 18951-18961.
75. Barroso, M.; Cowan, A. J.; Pendlebury, S. R.; Gratzel, M.; Klug, D. R.; Durrant, J. R., The Role of Cobalt Phosphate in Enhancing the Photocatalytic Activity of α-Fe_2O_3 toward Water Oxidation. *J. Am. Chem. Soc.* **2011,** *133*, 14868-14871.
76. Cummings, C. Y.; Marken, F.; Peter, L. M.; Tahir, A. A.; Wijayantha, K. G. U., Kinetics and mechanism of light-driven oxygen evolution at thin film α-Fe_2O_3 electrodes. *Chem. Commun.* **2012,** *48*, 2027-2029.
77. Ma, Y.; Le Formal, F.; Kafizas, A.; Pendlebury, S. R.; Durrant, J. R., Efficient suppression of back electron/hole recombination in cobalt phosphate surface-modified undoped bismuth vanadate photoanodes. *J. Mater. Chem. A* **2015,** *3*, 20649-20657.
78. Wang, L.; Mitoraj, D.; Turner, S.; Khavryuchenko, O. V.; Jacob, T.; Hocking, R. K.; Beranek, R., Ultrasmall CoO(OH)x Nanoparticles As a Highly Efficient " True " Cocatalyst in Porous Photoanodes for Water Splitting. *ACS Catalysis* **2017**, 4759-4767.
79. Dong, C.; Xing, M.; Zhang, J., Double-cocatalysts promote charge separation efficiency in CO_2 photoreduction: spatial location matters. *Mater. Horiz.* **2016,** *3*, 608-612.

Low temperature atomic layer deposition of cobalt oxide as an effective catalyst layer for photoelectrochemical water splitting devices

Table of Contents artwork